 CMES, vol.112, no.1, pp.1-32, 2016

Are "Higher-Order" and "Layer-wise Zig-Zag" Plate & Shell Theories Necessary for Functionally Graded Materials and Structures?

Yaping Zhang[1], Qifeng Fan[2], Leiting Dong[2,3] and Satya N. Atluri[4]

Abstract: Similar to the very vast prior literature on analyzing laminated composite structures, "higher-order" and "layer-wise higher-order" plate and shell theories for functionally-graded (FG) materials and structures are also widely popularized in the literature of the past two decades. However, such higher-order theories involve (1) postulating very complex assumptions for plate/shell kinematics in the thickness direction, (2) defining generalized variables of displacements, strains, and stresses, and (3) developing very complex governing equilibrium, compatibility, and constitutive equations in terms of newly-defined generalized kinematic and generalized kinetic variables. Their industrial applications are thus hindered by their inherent complexity, and the fact that it is difficult for end-users (front-line structural engineers) to completely understand all the newly-defined generalized DOFs for FEM in the higher-order and layer-wise theories. In an entirely different way, very simple 20-node and 27-node 3-D continuum solid-shell elements are developed in this paper, based on the simple theory of 3D solid mechanics, for static and dynamic analyses of functionally-graded plates and shells. A simple Over-Integration (a 4-point Gauss integration in the thickness direction) is used to evaluate the stiffness matrices of each element, while only a single element is used in the thickness direction without increasing the number of degrees of freedom. A stress-recovery approach is used to compute the distribution of transverse stresses by considering the equations of 3D elasticity in Cartesian as well as cylindrical polar coordinates. Comprehensive numerical results are presented for static and dynamic analyses of FG plates and shells, which agree well, either with the existing solutions in the published literature, or with the computationally very expensive solutions obtained by using simple 3D isoparametric elements (with standard Gauss Quadrature) available in NASTRAN (wherein many 3D elements are used

[1] Taizhou Polytechnic College, China.
[2] School of Aeronautic Science and Engineering, Beihang University, China.
[3] Corresponding Author, Email: dong.leiting@gmail.com
[4] Department of Mechanical Engineering, Texas Tech University, USA.

in the thickness direction to capture the varying material properties). The effects of the material gradient index, the span-to-thickness ratio, the aspect ratio and the boundary conditions are also studied in the solutions of FG structures. Because the proposed methodology merely involves: (2) standard displacement DOFs at each node, (2) involves a simple 4-point Gaussian over-integration in the thickness direction, (3) relies only on the simple theory of solid mechanics, and (4) is capable of accurately and efficiently predicting the static and dynamical behavior of FG structures in a very simple and cost-effective manner, it is thus believed by the authors that the painstaking and cumbersome development of "higher-order" or "layer-wise higher-order" theories is not entirely necessary for the analyses of FG plates and shells.

Keywords: functionally graded plates and shells, 20-node hexahedral element, 27-node hexahedral element, over-integration, higher order theory, layer-wise theory.

1 Introduction

Functionally graded materials (FGM) were proposed as heat-shielding structural materials by Japanese material scientists in 1984 [Koizumi (1997)]. Typically, FGMs are mixtures of ceramics and metals with material properties varying smoothly from one structural surface to another. In this way, thermal-stress concentrations developed at material interfaces of conventional structural components can be avoided. This excellent feature has promising applications for aircrafts, space vehicles, automobiles and other engineering structures. Thus, it is important to develop a simple and accurate tool for analyzing static and dynamic behaviors of FGM structures.

Similar to the very vast literature on laminated composite structures, specialized plate and shell theories for functionally-graded (FG) materials and structures were also extensively studied in the literature of the past two decades. These theories involve expanding the displacements using first-order, or higher-order power-series, or other types of functions, in the thickness direction of plates/shells. For example, the Kirchhoff and Reissner (or Mindlin) theories are the most widely-used plate/shell theories, see [Timoshenko and Woinowsky (1959), Reissner (1945) and Mindlin (1951)], which are embedded in almost every standard FEM packages such as Ansys, Abaqus, Nastran, etc. These and other first-order theories are also applied for static and dynamic analyses of FGM plates/shells, see [Zenkour (2006); Cheng and Batra (2000); Batra and Jin (2005)]. However, for relatively thick FGM structures, Kirchhoff and Reissner assumptions usually underestimate the deflections and overestimates natural frequencies, as transverse shear strains are

neglected (Kirchhoff) or assumed to be constant (Reissner) in such theories.

To overcome the aforementioned limitations, many higher-order shear deformation theories (HSDT) were later proposed, see [Lo, Christensen and Wu (1977); Reddy (1984); Reddy and Robbins (1994)], wherein the variations of in-plane displacements in the thickness direction are mostly approximated using third-order polynomials. These and other higher-order theories were used to analyze FGM plates and shells also, see [Reddy (2000); Qian, Batra and Chen (2004); Ferreira, Batra, Roque, Qian and Martins (2005)]. In [Carrera, Brischetto, Cinefra and Soave (2011)], it is also concluded that the normal deflection should also be expanded in the thickness direction to include the effects of thickness-stretching. Moreover, layer-wise theories, which expand displacements in each of many artificial layers of FGM plates/shells, were also used to improve the accuracy of the solution, see [Ramirez, Heyliger and Pan (2006); Carrera, Brischetto and Robaldo (2008)].

In order to derive higher-order or layer-wise theories of plates and shells, kinematic assumptions are substituted into the principle of potential energy of 3D elasticity. By exploring the stationarity conditions, very complex governing differential equations in terms of newly defined generalized displacements, strains and stresses can be derived, see [Reddy (2004)] for example. However, such complex differential equations cannot be directly solved. One usually goes back to derive the weak-forms of these governing differential equations, and thus develop the corresponding the finite element models to solve the problem numerically. In this sense, defining the many generalized displacements, strains, stresses, and deriving the complex higher-order or layer-wise theories and differential equations seems unnecessary. One can directly use the variational principle of 3D elasticity to develop finite elements for the modeling of plates and shells. Moreover, it is difficult for end-users to completely understand all the newly-defined generalized DOFs in higher-order theories (or their FEM counterparts), which have ambiguous physical meanings. Furthermore, it becomes very problematic when boundary conditions have to be enforced correctly for these generalized degrees of freedom, by the end-users.

In an entirely different way, [Dong, El-Gizawy, Juhany, Atluri (2014a,b)] directly developed 2D quadrilateral 4-node elements (for beam-type structures) , and 3D hexahedral 8-node finite elements (for plate and shell structures), for FG as well as laminated structures, based on the simple theories of 2D and 3D solid mechanics, respectively. Because the traditional displacement-based lowest order elements suffer from shear locking, a technique of locking-alleviation was used in Dong, El-Gizawy, Juhany, Atluri (2014a,b), by independently assuming locking-free element strains. Without using mixed variational principles, and thereby bypassing the troublesome LBB conditions of stability, a simple collocation method was used to satisfy the compatibility between the independently assumed strains and those de-

rived from the independently assumed displacement fields, at carefully selected required number of points inside the elements. Over-integration was also used in the thickness direction to accurately evaluate the stiffness matrix of FG and laminated elements. However, for very thick laminated structures with only a few layers, the computational accuracy is slightly compromised if only a single lowest-order finite element is used in the thickness direction. Therefore displacement-based higher-order solid (continuum) elements were also developed in [Fan, Zhang, Dong, Li, Atluri (2015)] for analyzing very thick laminates. Similarly, for FGM plates and shells, if the span-to-thickness ratio is very large, or if the material properties are varying in the thickness direction with very large gradients, it will be beneficial to have very simple higher-order displacements-based solid elements, with the standard displacement degrees of freedom, to improve the accuracy of solutions.

In this study, standard displacement-based 3D hexahedral 20-node element (DPH20) and a 3D 27-node element (DPH27), with over-integration in the thickness direction, are developed to carry out static and dynamic analyses of functionally graded plates and shells. Comprehensive numerical results are presented, which agree very well with existing solutions in the published literature, or with the computationally very-expensive solutions obtained by using standard 3D isoparametric element methodologies (with standard Gauss quadrature) available in commercial FEM codes. Because the proposed methodology: (1) merely involves the standard displacement DOFs at each node, (2) relies only on the simple theory of 3D solid mechanics, (3) simple 4-point Gauss quadrature in the thickness direction, and (4) is capable of accurately and efficiently predicting the static and dynamical behavior of FGM structures in a very simple and cost-effective manner, it is thus believed by the authors that the painstaking development of specialized "higher-order" or "layer-wise" theories is not entirely necessary for the analyses of FGM plates and shells. In the following sections, details of the proposed methodology are described and many numerical examples of various laminated plates/shells with different loads and boundary conditions are provided.

2 Formulation

2.1 Primal FEM with over-integration

As illustrated in Fig. 1, nodal shape functions of the 20-node and 27-node hexahedral elements can be defined in terms of local isoperimetric coordinates. We firstly define the following function for node i :

$$G_i = G(\xi_i, \eta_i, \zeta_i) = g(\xi_i, \xi) g(\eta_i, \eta) g(\zeta_i, \zeta) \tag{1}$$

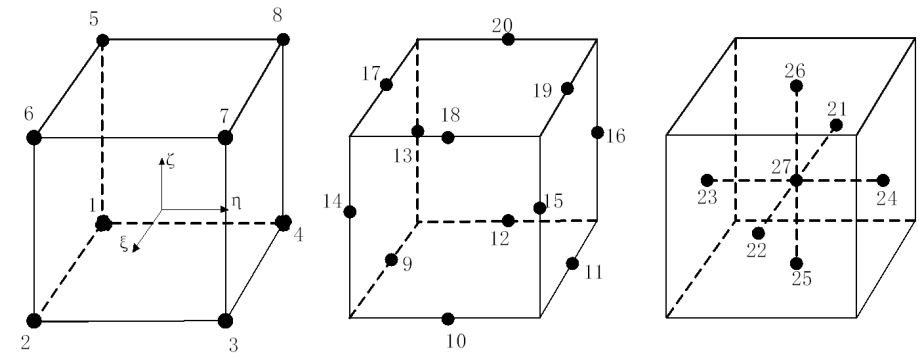

Figure 1: Numbering of nodes for 20-node/27-node hexahedral elements in ξ, η, ζcoordinates.

where ξ_i, η_i and ζ_i are the natural coordinates of node i, and $g(\xi_i, \xi)$, $g(\eta_i, \eta)$ and $g(\zeta_i, \zeta)$ are defined as:

$$\begin{cases} g(\xi_i, \xi) = \frac{1}{2}(1 + \xi_i \xi) & \text{if} \quad \xi_i = \pm 1 \\ g(\eta_i, \eta) = \frac{1}{2}(1 + \eta_i \eta) & \text{if} \quad \eta_i = \pm 1 \\ g(\zeta_i, \zeta) = \frac{1}{2}(1 + \zeta_i \zeta) & \text{if} \quad \zeta_i = \pm 1 \end{cases} \tag{2}$$

$$\begin{cases} g(\xi_i, \xi) = (1 - \xi^2) & \text{if} \quad \xi_i = 0 \\ g(\eta_i, \eta) = (1 - \eta^2) & \text{if} \quad \eta_i = 0 \\ g(\zeta_i, \zeta) = (1 - \zeta^2) & \text{if} \quad \zeta_i = 0 \end{cases} \tag{3}$$

Shape functions are therefore defined as follows.

For vertex nodes $i = 1, 2, \ldots, 8$:

$$N_i = G_i - \frac{G_e}{2} \tag{4}$$

where G_e for each vertex node is the sum of the G_i values of nodes on the three adjacent edges.

For mid-edge nodes $i = 9, 10, \ldots, 20$:

$$N_i = G_i \tag{5}$$

Nodal shape functions for the 27-node hexagonal element is slightly different, which can be found in most books of finite elements [Atluri (2005), Zienkiewicz and Taylor (1997)].

Thus the displacement fields within the element are interpolated by using nodal shape functions:

$$u_i = \sum_I N^{(I)} \tilde{u}_i^{(I)} \tag{6}$$

or in equivalent matrix-vector notations:

$$\mathbf{u} = \mathbf{N}\tilde{\mathbf{u}}^e \tag{7}$$

where $\tilde{\mathbf{u}}^e$ represents nodal displacements of the element.

Strain fields within the element are obtained by differentiating Eq. (7) with respect to Cartesian coordinates:

$$\boldsymbol{\varepsilon} = \mathbf{L}\mathbf{u} = \mathbf{L}\mathbf{N}\tilde{\mathbf{u}}^e = \mathbf{B}\tilde{\mathbf{u}}^e \tag{8}$$

where $\mathbf{L}$ is a linear differential operator.

By using the Galerkin Weak-Form or equivalent variational principles [Atluri (2005); Dong, Alotaibi, Mohiuddine and Atluri (2014c)], the element stiffness matrix and mass matrix are computed by:

$$\begin{aligned} \mathbf{k^e} &= \int_{\mathbf{\Omega^e}} \mathbf{B^T D B d\Omega} \\ \mathbf{m^e} &= \int_{\mathbf{\Omega^e}} \mathbf{N^T} \rho \mathbf{N d\Omega}. \end{aligned} \tag{9}$$

As discussed in [Dong, EI-Gizawy, Juhany and Atluri (2014b,c)], a scheme of over-integration in the thickness direction is used to evaluate the element stiffness and mass matrices for FGM. We know that for homogeneous materials, a $3\times3\times3$ Gauss integration is mostly used for evaluating Eq. (9). However, for FGM materials, the material properties are varying in the thickness direction, therefore the conventional $3\times3\times3$ Gauss integration will be insufficient. Thus, an increased-order integration, which is a 4-point Gauss integration in the thickness direction, is used to capture to varying material properties in the thickness direction.

The transverse normal and shear stresses are computed by using a stress-recovery approach considering the equilibrium equations of 3D linear elasticity. For the laminated plates, the distribution of transverse stresses can be obtained by numerically evaluating:

$$\begin{aligned} \sigma_{zx} &= -\int_{z_0}^{z} (\sigma_{xx,x} + \sigma_{xy,y}) dz \\ \sigma_{zy} &= -\int_{z_0}^{z} (\sigma_{yy,y} + \sigma_{xy,x}) dz \\ \sigma_{zz} &= -\int_{z_0}^{z} (\sigma_{zx,x} + \sigma_{zy,y}) dz \end{aligned} \tag{10}$$

where $z = z_0$ denote the lower surface of the plate.

For cylindrical shells, the distribution of transverse stresses can also be evaluated, by numerically solving the following 3 differential equations:

$$\begin{aligned}
&\frac{\partial \sigma_{r\theta}}{\partial r} + 2\frac{\sigma_{r\theta}}{r} = -\frac{1}{r}\frac{\partial \sigma_{\theta\theta}}{\partial \theta} - \frac{\partial \sigma_{\theta z}}{\partial z} \\
&\frac{\partial \sigma_{rz}}{\partial r} + \frac{\sigma_{rz}}{r} = -\frac{\partial \sigma_{zz}}{\partial z} - \frac{1}{r}\frac{\partial \sigma_{\theta z}}{\partial \theta} \\
&\frac{\partial \sigma_{rr}}{\partial r} + \frac{\sigma_{rr}}{r} = \frac{\sigma_{\theta\theta}}{r} - \frac{1}{r}\frac{\partial \sigma_{r\theta}}{\partial \theta} - \frac{\partial \sigma_{rz}}{\partial z}
\end{aligned} \tag{11}$$

In Eq. (11), the left hand-side involves stress components to be recovered, and the right-hand side are directly evaluated from the solutions of DPH20 or DPH27. Each equation is a first-order single-variable ODE, which can be solved with a variety of computational methods, see [Dong, Alotaibi, Mohiuddine and Atluri (2014c)]. In this study, simple collocation of Eq. (11) is implemented at a variety of points along the thickness direction. Combined with the traction free condition at the inner surface of the cylindrical shell, stress components $\sigma_{r\theta}, \sigma_{rz}, \sigma_{rr}$ can be efficiently recovered from the computed in-plane normal and shear stresses.

2.2 Functionally graded material properties

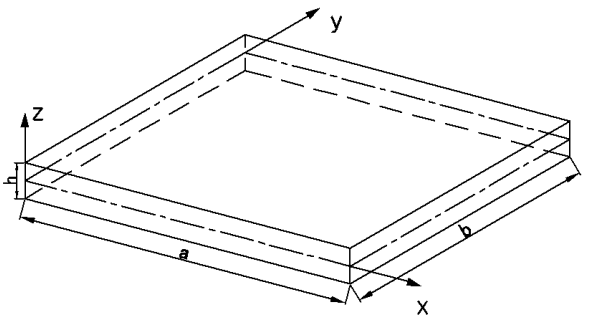

Figure 2: Geometry and the reference coordinate system for the FG plate.

We firstly consider a FG plate of length a, width b, and thickness h, as shown in Fig. 2. The x-, y-, and z-coordinates are along the length, width, and height directions of the plate, respectively. $z = 0$ is placed at the mid-surface of the plate.

The FG plate is mostly made by a mixture of two material phases, for example, a metal and a ceramic. The material properties of the FG plate, such as Young's

modulus E, mass density ρ and Poisson's ratio μ, are assumed to be varying continuously throughout the thickness of plate according to the power law distribution of volume fraction of constituents. According to the rule of mixtures, the effective material properties can be expressed as:

$$P = P_m V_m + P_c V_c = P_m (1 - V_c) + P_c V_c \tag{12}$$

where P_m, P_c, V_m and V_c are defined as the material properties and volume fractions of metal and ceramic, respectively.

In this paper, the volume fraction of ceramic is assumed to be subjected to the following power-law distribution along the thickness direction:

$$V_c = (\frac{z}{h} + \frac{1}{2})^p \tag{13}$$

where p is the material gradient index which should only be positive. Then the effective material properties of the FG plate can be expressed as:

$$\begin{cases} E(z) = (E_c - E_m)\left(\frac{2z+h}{2h}\right)^p + E_m \\ \mu(z) = (\mu_c - \mu_m)\left(\frac{2z+h}{2h}\right)^p + \mu_m \\ \rho(z) = (\rho_c - \rho_m)\left(\frac{2z+h}{2h}\right)^p + \rho_m \end{cases} \tag{14}$$

where the subscripts c and m represent ceramic and metal, respectively. The material properties of metals and ceramics used in this study are listed in Table 1.

Table 1: Material properties of metals and ceramics used in this study.

Material	Properties		
	E(GPa)	μ	ρ (kg/m^3)
Aluminum (Al)	70	0.3	2702
Alumina (Al_2O_3)	380	0.3	3800
Zirconia (ZrO_2)	200	0.3	5700
Silicon Nitride (Si_3N_4)	322.2715	0.24	2370
Stainless Steel (SUS304)	207.7877	0.31776	8166

As an example, the variation of Young's modulus E in the thickness direction of a FG Al/Al_2O_3 plate with various values of gradient index p is shown Fig.3. For p = 0

and p $= \infty$, the FG plate is purely ceramic (Al_2O_3) or metallic (Al), respectively. For other positive values of p, the material properties vary smoothly from metal-rich-surface to ceramic-rich surface with different gradients.

For functionally graded shells, material properties also vary smoothly from one surface to the other in the thickness direction, which is similar to the FGM plate.

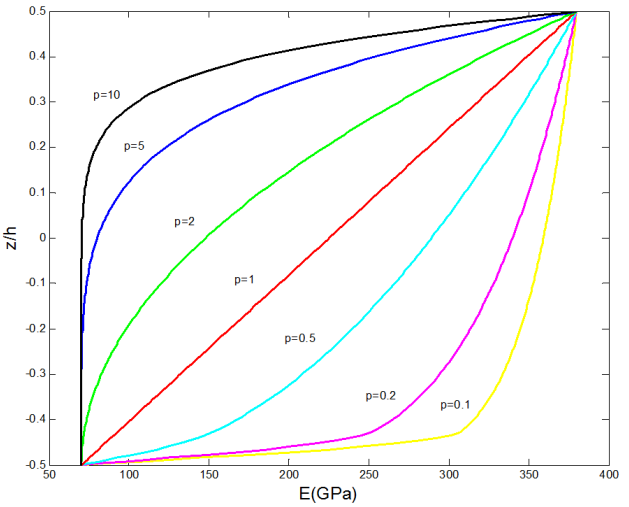

Figure 3: Variation of Young's modulus E through the dimensionless thickness (z/h) of Al/ Al_2O_3 plate.

3 Numerical Examples and Results

3.1 Static analysis

3.1.1 A simply-supported Al/Al_2O_3 FG plate subjected to a uniformly distributed lateral load

The first example studies a simply-supported thick-section Al/Al_2O_3 FG square plate subjected to a uniformly distributed lateral load: $q = 1GPa$. The plate is square with $a = b = 100$ mm, and the plate thickness is $h = 10$mm. Material parameters used for the FG plate are listed in Table 1. Three different gradient indexes ($p = 0.2,\ 2,\ 10$) are used.

We solve these problems using a uniform 10×10 mesh with DPH20 and DPH27 elements respectively, as well as using NASTRAN. We can see the difference of

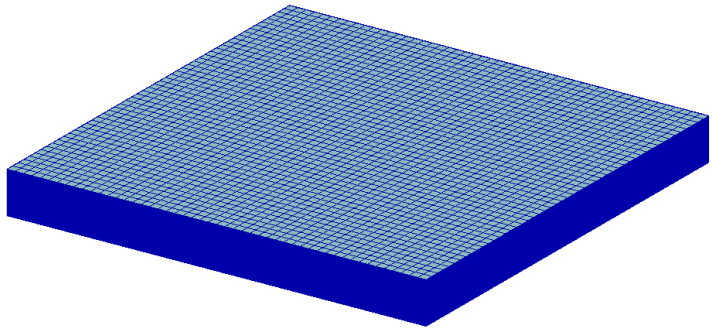

(a)

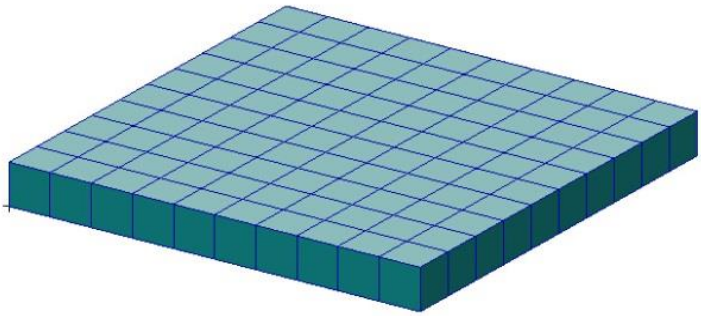

(b)

Figure 4: Finite element model for the FG plate (a/h = 10) by (a) NASTRAN and (b) the present DPH20/ DPH27 elements.

meshes between NASTRAN and the present DPH20/ DPH27 model in Fig. 4. When modeled by Nastran, it takes about half an hour to obtain the numerical results using 250,000 elements. In contrast, the present DPH20/ DPH27 model requires only 100 elements and about 15 seconds of computational time on a regular PC with i7 CPU. Computed in-plane and transverse shear stress are shown in Figs. 5-10, from which we can see that NASTRAN and the present method give similar results, though the computation time differs by two orders of magnitudes. Moreover, the DPH20 solution takes slightly less computational time than the DPH27 solution, as it contains a smaller number of DOFs. In fact, in all the following numerical examples, DPH20 always gives almost the same computational results as compared to DPH27, thus only results for DPH20 are demonstrated in the following subsections.

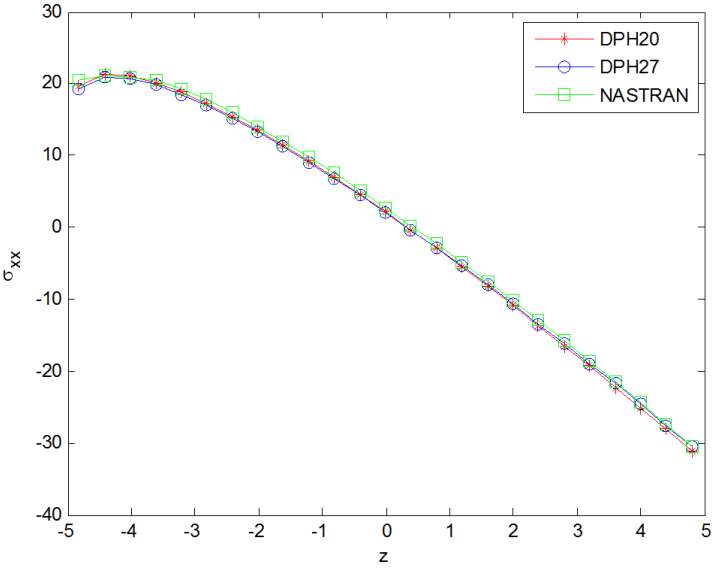

Figure 5: Computed in-plane normal stress σ_{xx} a t$x = y = 50mm$ for the thick-section Al/Al_2O_3 FG plate with gradient index $p = 0.2$.

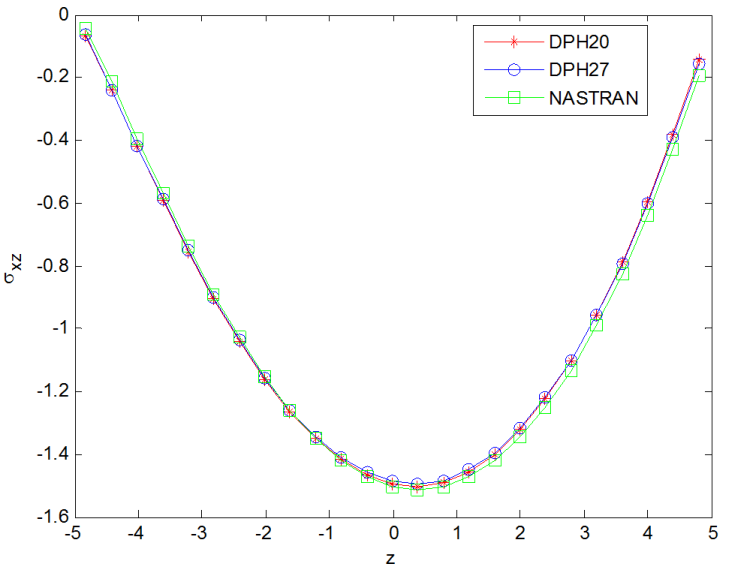

Figure 6: Computed transverse shear stress σ_{xz} at $x = y = 10mm$ for the thick-section Al/Al_2O_3 FG plate with gradient index $p = 0.2$.

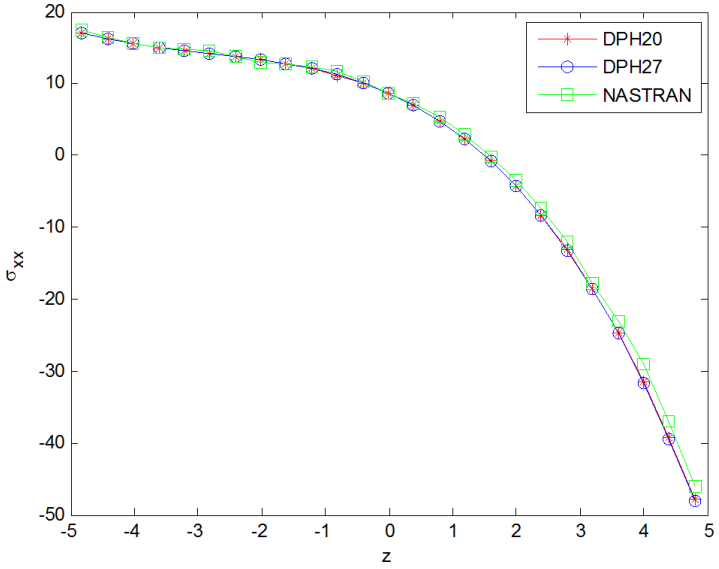

Figure 7: Computed in-plane normal stress σ_{xx} at $x = y = 50mm$ for the thick-section Al/Al_2O_3 FG plate with gradient index $p = 2$.

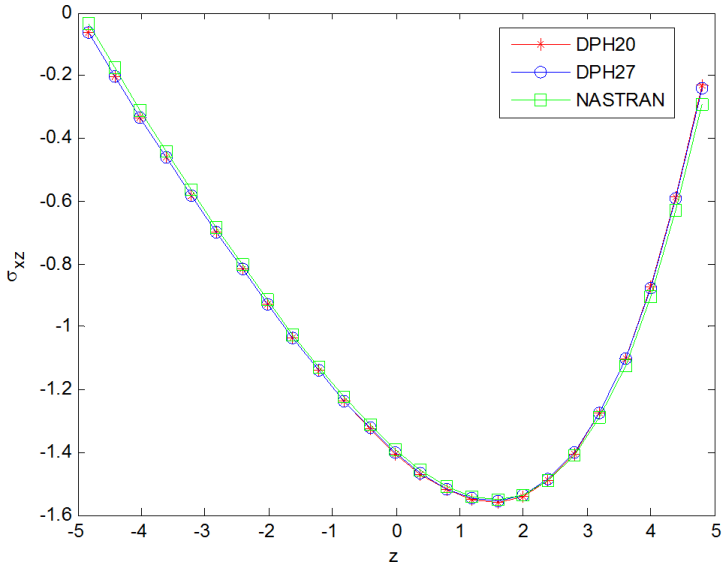

Figure 8: Computed transverse shear stress σ_{xz} at $x = y = 10mm$ for the thick-section Al/Al_2O_3 FG plate with gradient index $p = 2$.

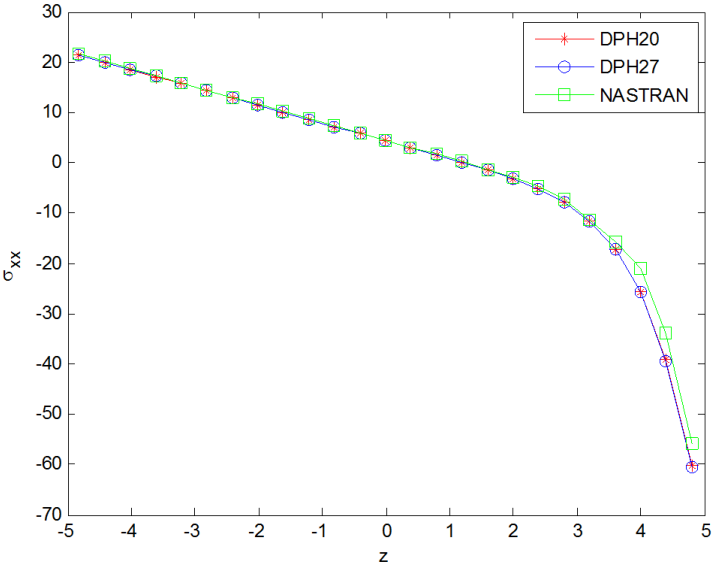

Figure 9: Computed in-plane normal stress σ_{xx} at $x = y = 50mm$ for the thick-section Al/Al_2O_3 FG plate with gradient index $p = 10$.

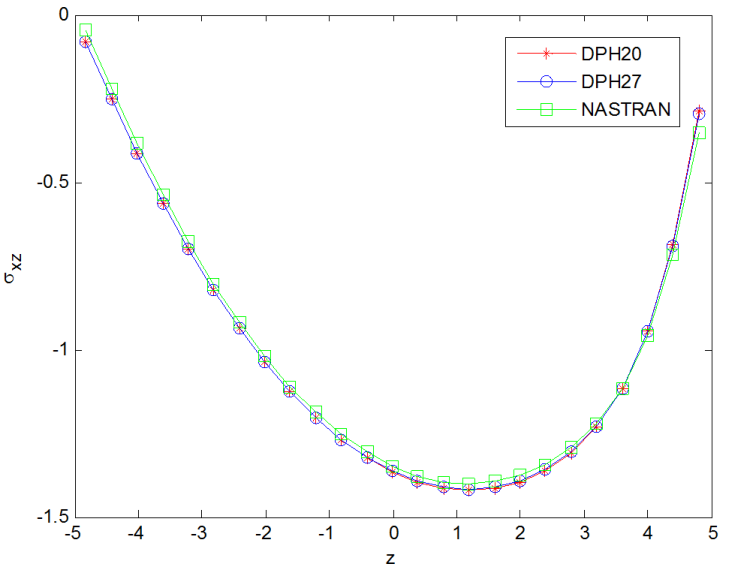

Figure 10: Computed transverse shear stress σ_{xz} at $x = y = 10mm$ for the thick-section Al/Al_2O_3 FG plate with gradient index $p = 10$.

3.1.2 A simply-supported Al/Al_2O_3 FG plate subjected to a uniform distributed lateral load

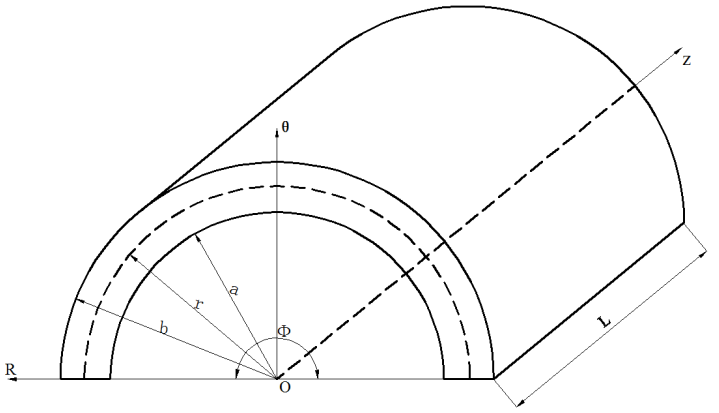

Figure 11: Geometry and coordinate system of a FG plate.

In this subsection, we consider a simply-supported thick-section Al/Al_2O_3 FG shell subjected to a uniformly distributed outer-pressure: $q = 1GPa$. Material parameters used in the FG plate are listed in Table 1. The inner radius and outer radius of the cylindrical shell are $r_{in} = 10mm$ and $r_{out} = 11mm$ respectively. The spans of the cylindrical shell in z direction and in θ direction are $l = 10mm$ and $\varphi = \pi$ respectively. The FG shell is simply supported at $\theta = 0, \pi$ and $z = 0, 10$.

We solve this problem using a uniform 60×20 mesh with DPH20 elements, as well as using NASTRAN (with 1.2 million DOFs), as shown in Fig. 12. Computed distributions of stresses are shown in Fig. 13. It can be clearly seen that the results by the present DPH20 elements agree well with those by NASTRAN even though DPH20 requires significantly less DOFs and computational time.

Figure 14: Mode shapes of simply-supported Al/Al_2O_3 square FG plates with a/h = 5 and p=1.

3.2 Free vibration analysis

3.2.1 Modal analysis of functionally graded plates

Simply-supported Al/Al_2O_3 square FG plates with various gradient indexes are analyzed in this subsection. Material parameters used in the FG plates are listed in Table 1. The span-to-thickness ratio a/h = 10 is adopted in the example. The non-dimensional frequency parameters $\overline{\omega}_n = \omega_n a^2/h\sqrt{\rho_c/E_c}$ are used to compare

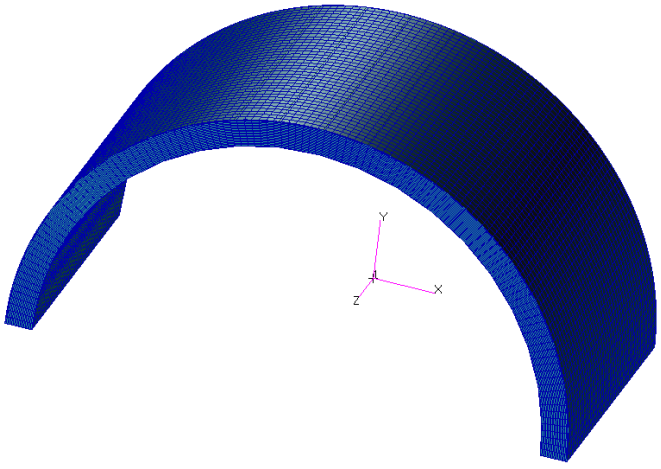

(a)

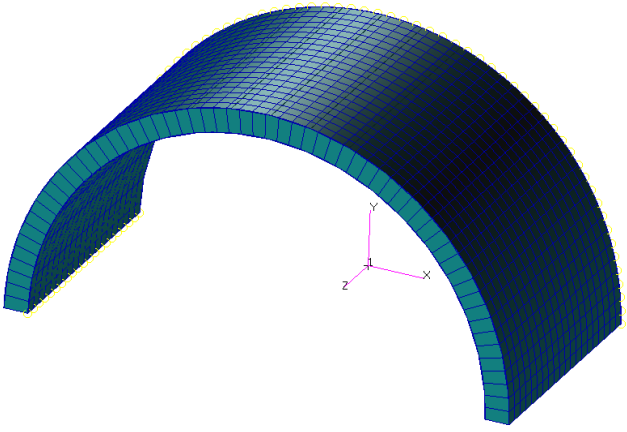

(b)

Figure 12: Finite element model for the FG shell by (a) NASTRAN and (b) the present DPH20 elements.

results obtained in this paper to the results in the literatures. We solve this problem using a uniform 20×20 mesh with DPH20 elements. The present results are shown in Table 2 along with the exact solution by [Jin, Su, Shi, Ye and Gao (2014)] and the solution by a variational Ritz method [Huang, McGee and Wang (2013)]. It is seen that the DPH20 solution agrees well with the exact solution of 3D elasticity to a satisfactory precision.

We then consider extremely thick simply-supported Al/Al_2O_3 square FG plates

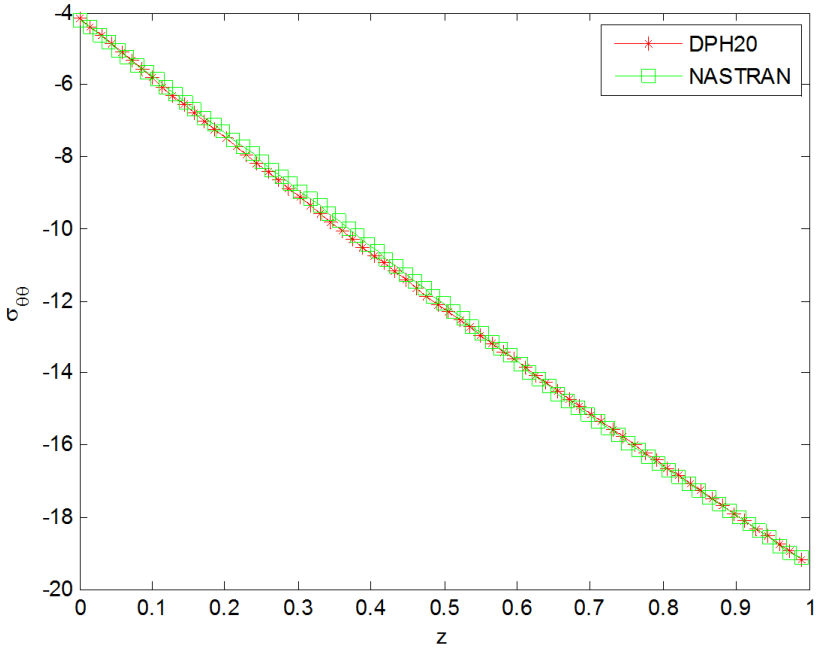
DPH20
NASTRAN
σθθ
z
-4
-6
-8
-10
-12
-14
-16
-18
-20
0
0.1
0.2
0.3
0.4
0.5
0.6
0.7
0.8
0.9
1

(a)

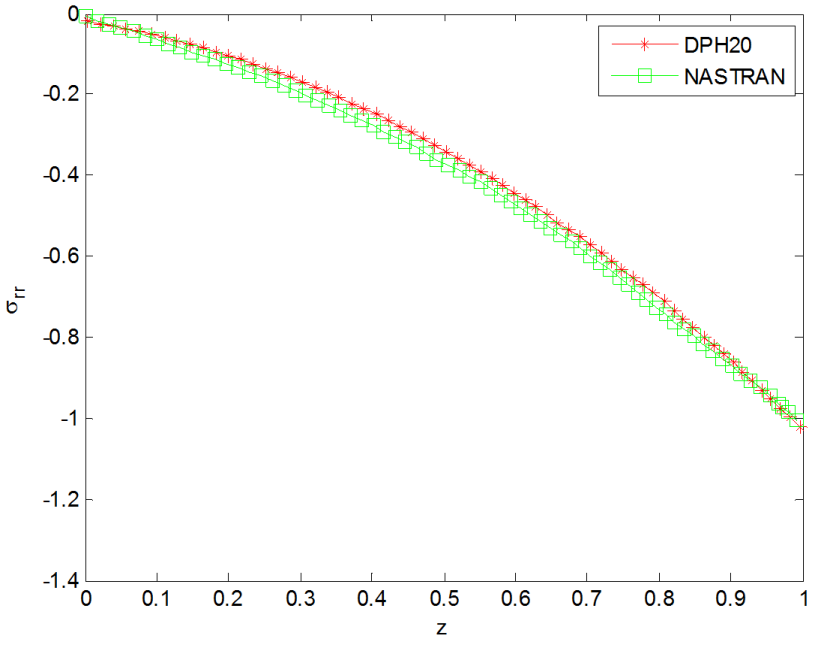
DPH20
NASTRAN
σrr
z
0
-0.2
-0.4
-0.6
-0.8
-1
-1.2
-1.4
0
0.1
0.2
0.3
0.4
0.5
0.6
0.7
0.8
0.9
1

(b)

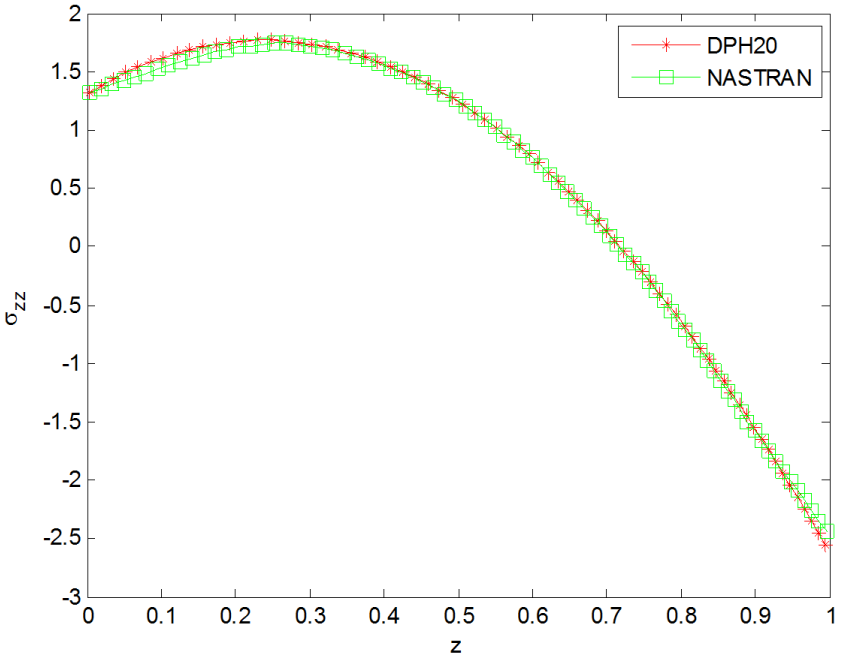

(c)

Figure 13: Computed $\sigma_{\theta\theta}, \sigma_{rr}, \sigma_{zz}$ at $\theta = \frac{61}{120}\pi, z = 5mm$ for the thick-section Al/Al_2O_3 FG plate.

with span-to-thickness ratio $a/h = 5$. Two different kinds of meshes with $20\times20\times1$ and $20\times20\times2$ DPH20 elements (one or two layers of elements in the thickness direction) are used. The first five non-dimensional frequency parameters $\overline{\omega}_n = \omega_n a^2/h\sqrt{\rho_c/E_c}$ are presented in Table 3. Although both models give acceptable solutions, more accurate results are obtained by using two layers of elements (3.33% and 0.12% maximum errors for $20\times20\times1$ and $20\times20\times2$ meshes respectively). Therefore, a uniform $20\times20\times2$ mesh with DPH20 elements will be used if the FG plate is extremely thick (i.e. $a/h \leq 5$) in the following numerical examples.

Simply-supported Al/Al_2O_3 square FG plates with span-to-thickness ratio varied from 5 to 20 and gradient index varied from 0 to 10 are analyzed to verify the accuracy and ef?cient of the present method. The non-dimensional frequency parameters $\overline{\omega}_n = \omega_n/h\sqrt{\rho_c/E_c}$ obtained using the DPH20 element are compared with HSDT solutions [Thai, Park and Choi (2013); Hosseini-Hashemi, Fadaee and Atashipour (2011a); Matsunaga (2008)], FSDT solutions [Hosseini-Hashemi, Fadaee

Table 2: The non-dimensional frequency parameters $\overline{\omega}_n = \omega_n a^2/h\sqrt{\rho_c/E_c}$ of the simply-supported Al/Al2O3 square FG plates with a/h=10.

p	Method	$\overline{\omega}_n$				
		1	2	3	4	5
0	Jin et al. (2014)	5.779	13.810	13.810	19.480	19.480
	Huang et al. (2013)	5.777	13.810	13.810	19.480	19.480
	DPH20	5.795	13.898	13.898	19.483	19.483
1	Jin et al. (2014)	4.428	10.630	10.630	16.200	16.200
	Huang et al. (2013)	4.426	10.630	10.630	16.200	16.200
	DPH20	4.434	10.668	10.668	16.202	16.202
5	Jin et al. (2014)	3.774	8.931	8.931	12.640	12.640
	Huang et al. (2013)	3.772	8.927	8.927	12.640	12.640
	DPH20	3.795	9.047	9.047	12.642	12.642

Table 3: The non-dimensional frequency parameters $\overline{\omega}_n = \omega_n a^2/h\sqrt{\rho_c/E_c}$ of simply-supported Al/Al2O3 square FG plates with a/h=5.

p	Method	$\overline{\omega}_n$				
		1	2	3	4	5
0	Jin et al. (2014)	5.304	9.742	9.742	11.650	11.650
	Huang et al. (2013)	5.304	9.742	9.742	11.650	11.650
	20×20×1 elements	5.356	9.742	9.742	11.849	11.849
	20×20×2 elements	5.307	9.742	9.742	11.664	11.664
1	Jin et al. (2014)	4.100	8.089	8.089	9.108	9.108
	Huang et al. (2013)	4.099	8.089	8.089	9.107	9.107
	20×20×1 elements	4.123	8.090	8.090	9.201	9.201
	20×20×2 elements	4.101	8.089	8.089	9.118	9.118
5	Jin et al. (2014)	3.405	6.296	6.296	7.344	7.344
	Huang et al. (2013)	3.405	6.296	6.296	7.343	7.343
	20×20×1 elements	3.470	6.304	6.304	7.589	7.589
	20×20×2 elements	3.406	6.296	6.296	7.352	7.352

and Atashipour (2011b); Zuo, Yang, Chen, Xie and Zhang (2014)] and CPT solutions [Thai, Park and Choi (2013)] in Table 4. Obviously, the solutions given by the proposed DPH20 element are in excellent agreement with the HSDT solutions [Thai, Park and Choi (2013); Hosseini-Hashemi, Fadaee and Atashipour (2011a); Matsunaga (2008)] and FSDT solutions [Hosseini-Hashemi, Fadaee and Atashipour (2011b); Zuo, Yang, Chen, Xie and Zhang (2014)]. The results also indicate that the CPT over-predicts the natural frequency of FG plates, especially for the thick plate at higher modes of vibration. Moreover, it is found that the non-dimensional frequency parameter decreases as the gradient index increases. This is because larger gradient index leads to decrease of stiffness. The mode shapes of simply-supported Al/Al_2O_3 square FG plates with a/h = 5 and 10 are depicted in Figs. 14 and 15, respectively.

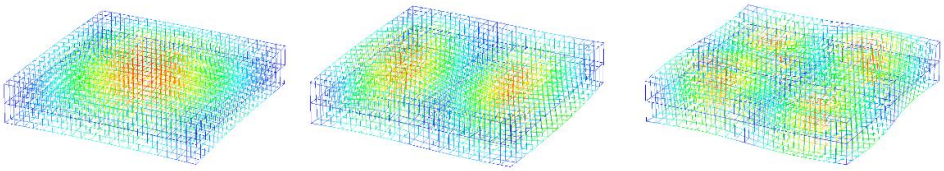

(a) Mode (1, 1) (b) Mode (1, 2) (c) Mode (2, 2)

Figure 14: Mode shapes of simply-supported Al/Al2O3 square FG plates with a/h = 5 and p=1.

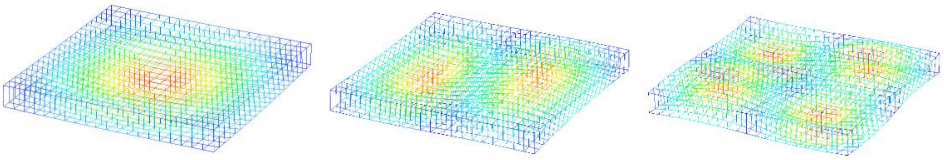

(a) Mode (1, 1) (b) Mode (1, 2) (c) Mode (2, 2)

Figure 15: Mode shapes of simply-supported Al/Al2O3 square FG plates with a/h = 10 and p=1.

In Table 5, the non-dimensional fundamental frequency parameters $\overline{\omega} = \omega/h\sqrt{\rho_m/E_m}$ of Al/ZrO_2 rectangular FG plates with different boundary conditions are presented. There are five different sets of boundary conditions, namely, SSSS (simply supported at all edges), SCSC (clamped at $x = 0, a$ and simply supported at $y = 0, b$), SCSF (clamped at $x = 0$, simply supported at $y = 0, b$ and free at $x = a$), SSSC (clamped

Table 4: The non-dimensional frequency parameters $\overline{\omega}_n = \omega_n / h\sqrt{\rho_c / E_c}$ of simply-supported Al/Al2O3 square FG plates.

a/h	Mode no. (m, n)	Method	p				
			0	0.5	1	4	10
5	(1, 1)	Hosseini-Hashemi et al. (2011a)	0.2113	0.1807	0.1631	0.1378	0.1301
		Thai et al. (2013)	0.2113	0.1807	0.1631	0.1378	0.1301
		Matsunaga (2008)	0.2121	0.1819	0.1640	0.1383	0.1306
		Hosseini-Hashemi et al. (2011b)	0.2112	0.1805	0.1631	0.1397	0.1324
		Zuo et al. (2014)	0.2112	0.1802	0.1625	0.1384	0.1315
		CPT	0.2314	0.1959	0.1762	0.1524	0.1467
		present	0.2123	0.1818	0.1640	0.1383	0.1307
	(1, 2)	Hosseini-Hashemi et al. (2011a)	0.4623	0.3989	0.3607	0.2980	0.2771
		Thai et al. (2013)	0.4623	0.3989	0.3607	0.2980	0.2771
		Matsunaga (2008)	0.4658	0.4040	0.3644	0.3000	0.2790
		Hosseini-Hashemi et al. (2011b)	0.4618	0.3978	0.3604	0.3049	0.2856
		Zuo et al. (2014)	0.4618	0.3986	0.3625	0.3107	0.2865
		CPT	0.5535	0.4681	0.4198	0.3603	0.3481
		present	0.4665	0.4033	0.3647	0.3002	0.2796
	(2, 2)	Hosseini-Hashemi et al. (2011a)	0.6688	0.5803	0.5254	0.4284	0.3948
		Thai et al. (2013)	0.6688	0.5803	0.5254	0.4284	0.3948
		Matsunaga (2008)	0.6753	0.5891	0.5444	0.4362	0.3981
		Hosseini-Hashemi et al. (2011b)	0.6676	0.5779	0.5245	0.4405	0.4097
		Zuo et al. (2014)	0.6676	0.5779	0.5248	0.4401	0.4090
		CPT	0.8504	0.7184	0.6425	0.5478	0.5306
		present	0.6767	0.5885	0.5333	0.4329	0.3994

10	(1, 1)	Hosseini-Hashemi et al. (2011a)	0.0577	0.0490	0.0442	0.0381	0.0364
		Thai et al. (2013)	0.0577	0.0490	0.0442	0.0381	0.0364
		Matsunaga (2008)	0.0578	0.0492	0.0443	0.0381	0.0364
		Hosseini-Hashemi et al. (2011b)	0.0577	0.0490	0.0442	0.0382	0.0366
		Zuo et al. (2014)	0.0577	0.0491	0.0443	0.0384	0.0367
		CPT	0.0592	0.0502	0.0452	0.0392	0.0377
		present	0.0579	0.0493	0.0443	0.0383	0.0365
	(1, 2)	Hosseini-Hashemi et al. (2011a)	0.1377	0.1174	0.1059	0.0903	0.0856
		Thai et al. (2013)	0.1377	0.1174	0.1059	0.0903	0.0856
		Matsunaga (2008)	0.1381	0.1180	0.1063	0.0904	0.0859
		Hosseini-Hashemi et al. (2011b)	0.1376	0.1173	0.1059	0.0911	0.0867
		Zuo et al. (2014)	0.1376	0.1171	0.1055	0.0903	0.0864
		CPT	0.1464	0.1239	0.1115	0.0966	0.0930
		present	0.1390	0.1187	0.1067	0.0914	0.0869
	(2, 2)	Hosseini-Hashemi et al. (2011a)	0.2113	0.1807	0.1631	0.1378	0.1301
		Thai et al. (2013)	0.2113	0.1807	0.1631	0.1378	0.1301
		Matsunaga (2008)	0.2121	0.1819	0.1640	0.1383	0.1306
		Hosseini-Hashemi et al. (2011b)	0.2112	0.1805	0.1631	0.1397	0.1324
		Zuo et al. (2014)	0.2112	0.1808	0.1638	0.1405	0.1327
		CPT	0.2314	0.1959	0.1762	0.1524	0.1467
		present	0.2141	0.1832	0.1648	0.1404	0.1331
20	(1, 1)	Hosseini-Hashemi et al. (2011a)	0.0148	0.0125	0.0113	0.0098	0.0094
		Thai et al. (2013)	0.0148	0.0125	0.0113	0.0098	0.0094
		Hosseini-Hashemi et al. (2011b)	0.0148	0.0125	0.0113	0.0098	0.0094
		Zuo et al. (2014)	0.0148	0.0126	0.0114	0.0099	0.0095
		CPT	0.0149	0.0126	0.0114	0.0099	0.0095
		present	0.0148	0.0125	0.0113	0.0098	0.0094

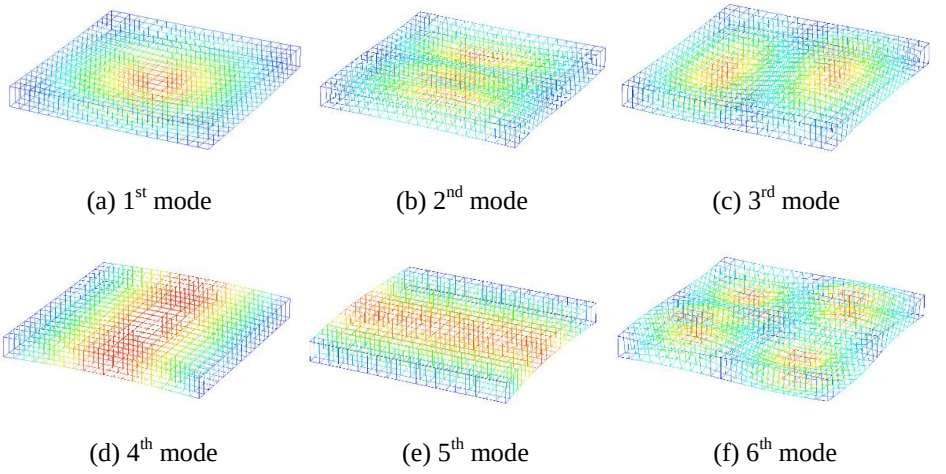

(a) 1st mode (b) 2nd mode (c) 3rd mode

(d) 4th mode (e) 5th mode (f) 6th mode

Figure 16: First six mode shapes of a SSSS Al/ZrO2 square FG plates with a/h = 10 and p=1.

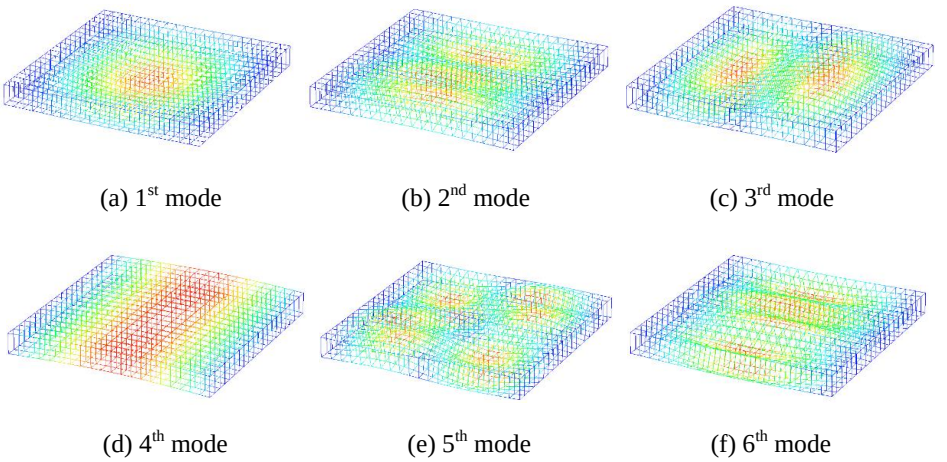

(a) 1st mode (b) 2nd mode (c) 3rd mode

(d) 4th mode (e) 5th mode (f) 6th mode

Figure 17: First six mode shapes of a SCSC Al/ZrO2 square FG plates with a/h = 10 and p=1.

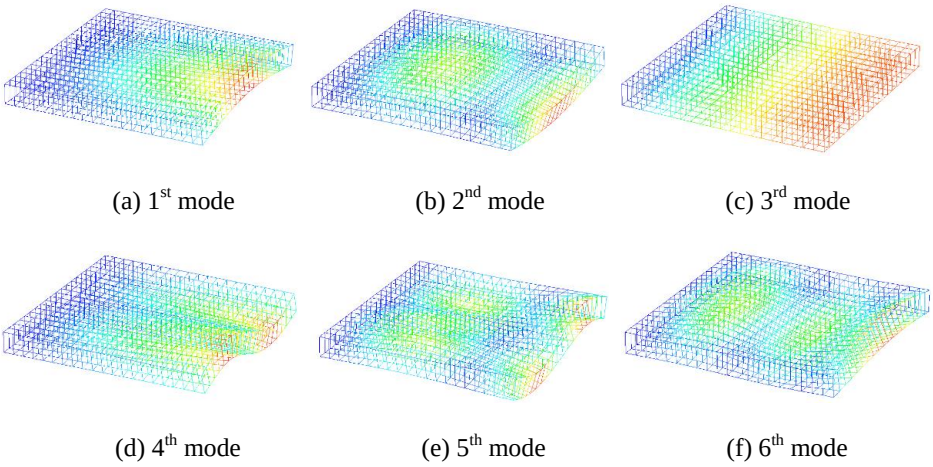

(a) 1st mode (b) 2nd mode (c) 3rd mode

(d) 4th mode (e) 5th mode (f) 6th mode

Figure 18: First six mode shapes of a SCSF Al/ZrO2 square FG plates with a/h = 10 and p=1.

at $x = 0$ and simply supported at $x = a, y = 0, b$) and SSSF (simply supported at $x = 0, y = 0, b$ and free at $x = a$). The results obtained by the present method with various values of aspect ratio (b/a = 1 and 2), span-to-thickness ratio (a/h = 5 and 10) and gradient index (p = 0, 1, 2 and 5) are compared with exact solutions reported in [Jin, Su, Shi, Ye and Gao (2014)]. Very good agreement is observed for all the computations, and the difference of the frequency parameters does not exceed 0.91% for the worst case. The first six 3D mode shapes of SSSS, SCSC and SCSF Al/ZrO_2 square FG plates are shown in Figs. 16–18.

3.2.2 Modal analysis of functionally graded shells

In this subsection, a clamped FG cylindrical shell is studied with geometric parameters $a/h = 10$, *a/R = 0.1*, $a = b$ and with different gradient indexes from 0 to ∞. The constituents of the FG shell considered in this example are Si_3N_4 and SUS304, whose material properties are given in Table 1. The non-dimensional frequency parameter adopted for comparison is $\overline{\omega}_n = \omega_n a^2 \sqrt{\rho_m h / D_m}$ in which $D_m = E_m h^3 / 12(1 - \nu_m^2)$. We solve these problems using a uniform 20×20×1 mesh with DPH20 elements. The first four non-dimensional frequency parameters are presented in Table 6 along with HSDT solutions [Neves, Ferreira, Carrera, Cinefra, Roque, Jorge and Soares (2013); Pradyumna and Bandyopadhyay (2008); Yang and Shen (2003)]. From Table 6, it is found that the solutions given by the proposed DPH20 element are in excellent agreement with the HSDT solutions.

Table 5: The non-dimensional fundamental frequency parameters $\overline{\omega} = \omega/h\sqrt{\rho_m/E_m}$ of Al/ZrO_2 rectangular FG plates with different boundary conditions.

b/a	a/h	p	SSSS		SCSC		SCSF		SSSC		SSSF	
			Jin et al. (2014)	present	Jin et al. (2014)	present	Jin et al. (2014)	present	Jin et al. (2014)	present	Jin et al. (2014)	present
1	10	0	0.0673	0.0674	0.0950	0.0957	0.0432	0.0434	0.0793	0.0797	0.0401	0.0402
		1	0.0620	0.0621	0.0878	0.0883	0.0398	0.0399	0.0732	0.0734	0.0369	0.0370
		2	0.0617	0.0619	0.0872	0.0879	0.0397	0.0398	0.0728	0.0732	0.0368	0.0369
		5	0.0629	0.0632	0.0882	0.0890	0.0405	0.0407	0.0740	0.0741	0.0376	0.0377
	5	0	0.2469	0.2470	0.3200	0.3197	0.1607	0.1607	0.2803	0.2802	0.1510	0.1511
		1	0.2285	0.2286	0.2981	0.2978	0.1486	0.1486	0.2602	0.2601	0.1395	0.1396
		2	0.2264	0.2266	0.2934	0.2930	0.1475	0.1475	0.2570	0.2569	0.1386	0.1387
		5	0.2281	0.2282	0.2916	0.2911	0.1489	0.1489	0.2572	0.2571	0.1403	0.1404
2	10	0	0.0426	0.0426	0.0470	0.0471	0.0360	0.0360	0.0445	0.0446	0.0356	0.0356
		1	0.0392	0.0392	0.0433	0.0433	0.0331	0.0332	0.0410	0.0410	0.0327	0.0328
		2	0.0391	0.0391	0.0432	0.0432	0.0330	0.0331	0.0408	0.0409	0.0327	0.0327
		5	0.0399	0.0400	0.0440	0.0441	0.0337	0.0338	0.0417	0.0418	0.0333	0.0334
	5	0	0.1607	0.1607	0.1742	0.1741	0.1134	0.1134	0.1667	0.1667	0.1134	0.1134
		1	0.1484	0.1484	0.1611	0.1609	0.1085	0.1085	0.1540	0.1540	0.1085	0.1085
		2	0.1474	0.1474	0.1598	0.1596	0.1059	0.1059	0.1529	0.1529	0.1059	0.1059
		5	0.1492	0.1493	0.1613	0.1611	0.1024	0.1024	0.1546	0.1545	0.1024	0.1024

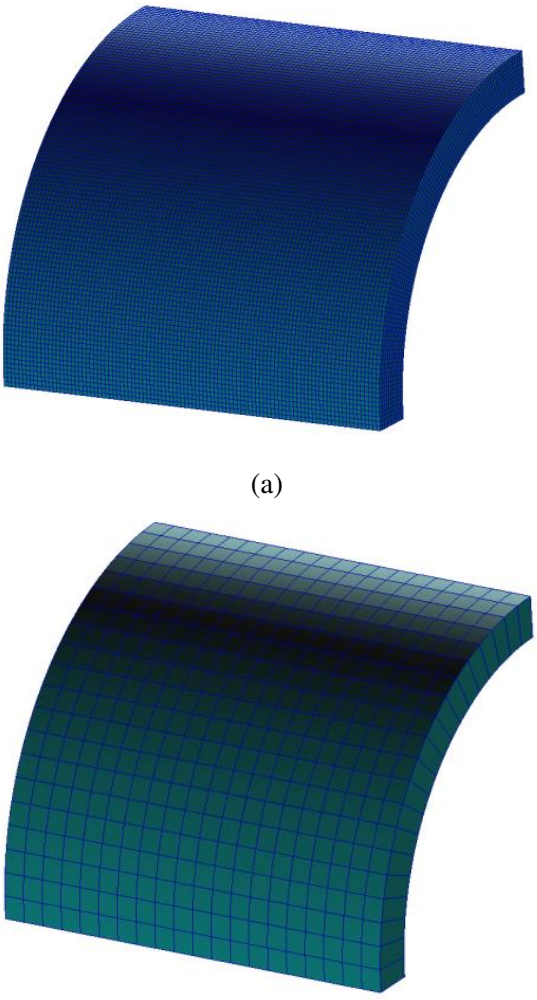

(a)

(b)

Figure 19: Finite element model for the FG cylindrical shell by (a) NASTRAN and (b) the present DPH20 elements.

We also consider FG cylindrical shells with different boundary conditions. The constituents of the FG shell are Si_3N_4 and SUS304, whose material properties are given in Table 1. The gradient index $p = 2$ is used in this example. The inner radius and outer radius of the cylindrical shell are $r_{in} = 60mm$ and $r_{out} = 70mm$ respectively. The spans of the cylindrical shell in z direction and in θ direction are

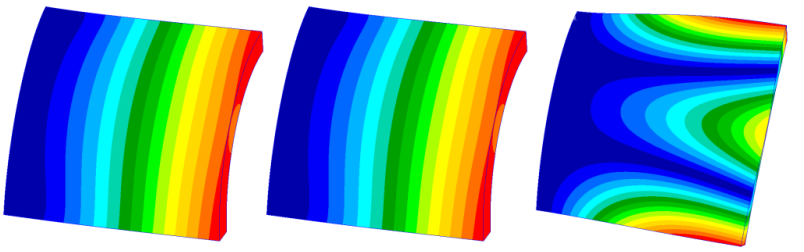

(a) $\overline{\omega}_1$ **=0.0832** $\overline{\omega}_2$ **=0.1003** $\overline{\omega}_3$ **=0.2793**

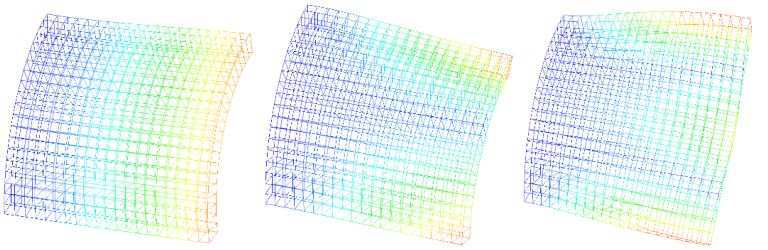

(b) $\overline{\omega}_1$ **=0.0835** $\overline{\omega}_2$ **=0.1011** $\overline{\omega}_3$ **=0.2813**

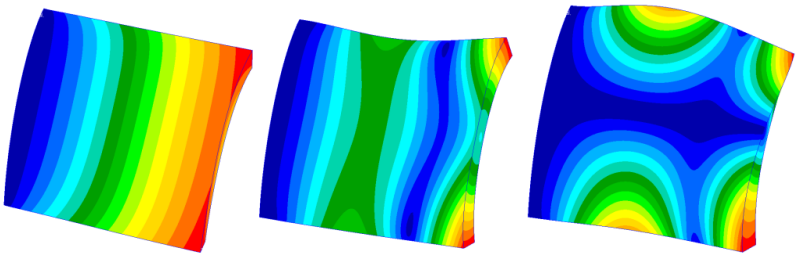

(a) $\overline{\omega}_4$ **=0.2815** $\overline{\omega}_5$ **=0.3586** $\overline{\omega}_6$ **=0.3611**

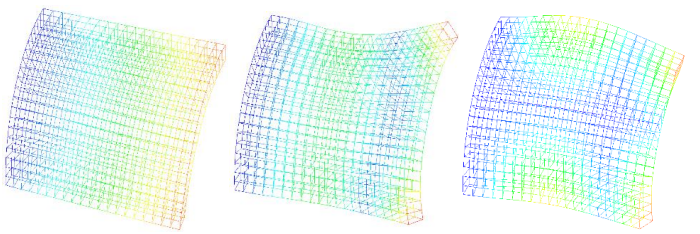

(b) $\overline{\omega}_4$ **=0.2820** $\overline{\omega}_5$ **=0.3610** $\overline{\omega}_6$ **=0.3649**

Figure 20: First six non-dimensional frequency parameters and their corresponding mode shapes of a CFFF FG cylindrical shell by (a) NASTRAN and (b) the present DPH20 elements.

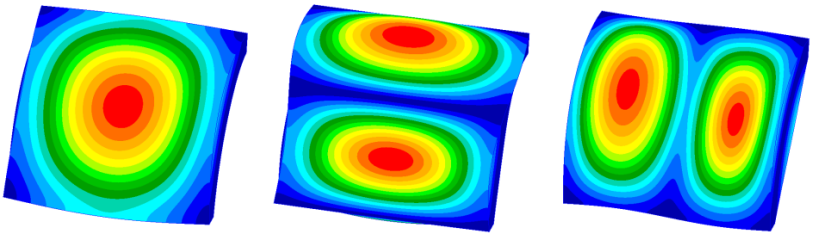

(a) $\overline{\omega}_1$ **=0.3442** $\overline{\omega}_2$ **=0.5107** $\overline{\omega}_3$ **=0.7114**

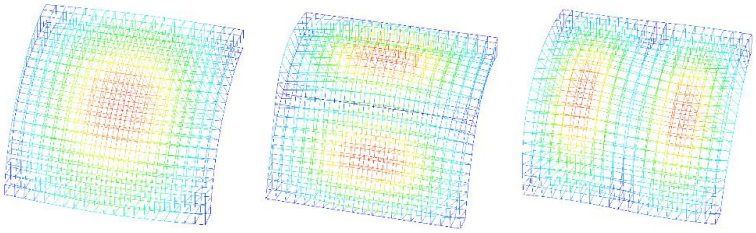

(b) $\overline{\omega}_1$ **=0.3450** $\overline{\omega}_2$ **=0.5156** $\overline{\omega}_3$ **=0.7151**

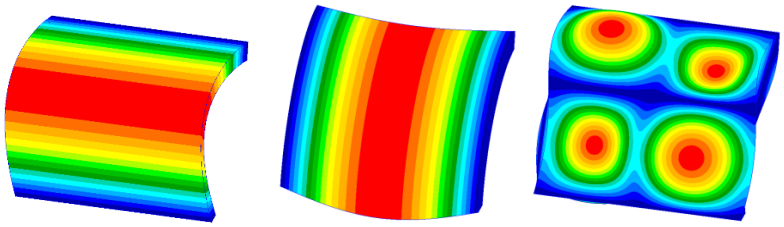

(a) $\overline{\omega}_4$ **=0.7860** $\overline{\omega}_5$ **=0.8221** $\overline{\omega}_6$ **=0.8540**

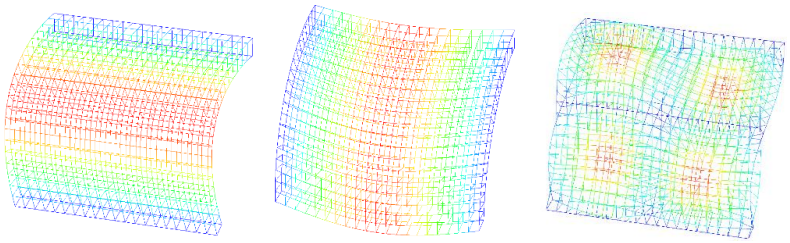

(b) $\overline{\omega}_4$ **=0.7865** $\overline{\omega}_5$ **=0.8229** $\overline{\omega}_6$ **=0.8636**

Figure 21: First six non-dimensional frequency parameters and their corresponding mode shapes of a SSSS FG cylindrical shell by (a) NASTRAN and (b) the present DPH20 elements.

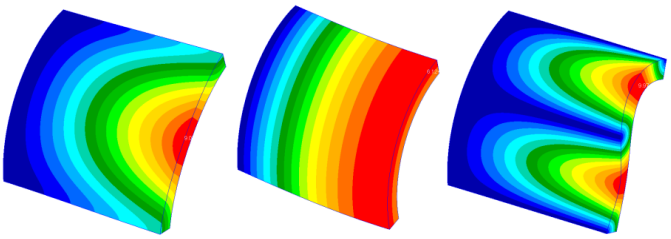

(a) $\overline{\omega}_1$ **=0.1732** $\overline{\omega}_2$ **=0.4113** $\overline{\omega}_3$ **=0.4229**

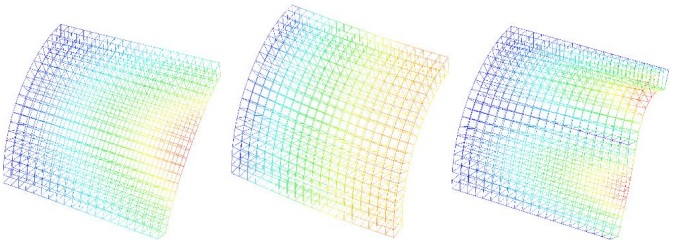

(b) $\overline{\omega}_1$ **=0.1739** $\overline{\omega}_2$ **=0.4117** $\overline{\omega}_3$ **=0.4272**

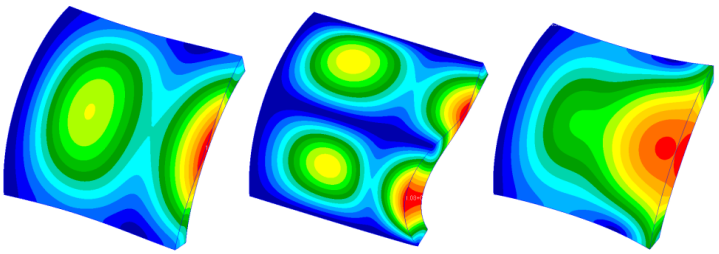

(a) $\overline{\omega}_4$ **=0.5030** $\overline{\omega}_5$ **=0.6505** $\overline{\omega}_6$ **=0.8826**

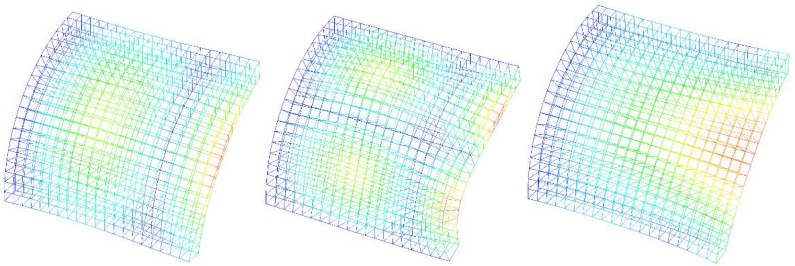

(b) $\overline{\omega}_4$ **=0.5061** $\overline{\omega}_5$ **=0.6593** $\overline{\omega}_6$ **=0.8838**

Figure 22: First six non-dimensional frequency parameters and their corresponding mode shapes of a CFFF FG cylindrical shell by (a) NASTRAN and (b) the present DPH20 elements.

Table 6: The non-dimensional frequency parameter $\overline{\omega}_n = \omega_n a^2\sqrt{\rho_m h/D_m}$ of clamped FG cylindrical shells.

Mode	Method	p = 0	p = 0.2	p = 2	p = 10	p = ∞
1	Pradyumna et al. (2008)	72.9613	60.0269	39.1457	33.3666	32.0274
	Yang et al. (2003)	74.5180	57.4790	40.7500	35.8520	32.7610
	Neves et al. (2013)[a]	74.2634	60.0061	40.5259	35.1663	32.6108
	Neves et al. (2013)[b]	74.5821	60.3431	40.8262	35.4229	32.8593
	present	75.5192	61.7080	41.3946	35.8943	33.4029
2	Pradyumna et al. (2008)	138.5552	113.8806	74.2915	63.2869	60.5546
	Yang et al. (2003)	144.6630	111.7170	78.8170	69.0750	63.3140
	Neves et al. (2013)[a]	141.6779	114.3788	76.9725	66.6482	61.9329
	Neves et al. (2013)[b]	142.4281	115.2134	77.6639	67.1883	62.4886
	present	144.9942	118.3963	79.1736	68.5137	63.8204
3	Pradyumna et al. (2008)	138.5552	114.0266	74.3868	63.3668	60.6302
	Yang et al. (2003)	145.7400	112.5310	79.4070	69.6090	63.8060
	Neves et al. (2013)[a]	141.8485	114.5495	77.0818	66.7332	62.0082
	Neves et al. (2013)[b]	142.6024	115.3665	77.7541	67.2689	62.5668
	present	145.1461	118.5338	79.2588	68.5822	63.8848
4	Pradyumna et al. (2008)	195.5366	160.6235	104.7687	89.1970	85.1788
	Yang et al. (2003)	206.9920	159.8550	112.4570	98.3860	90.3700
	Neves et al. (2013)[a]	199.1566	160.7355	107.9484	93.3350	86.8160
	Neves et al. (2013)[b]	200.3158	162.0337	108.9677	94.0923	87.6341
	present	204.4336	166.8808	111.3657	96.2167	89.6707

$l = 100mm$ and $\phi = \pi/2$ respectively.

Three different boundary conditions are studied which are CFFF, SSSS and CSSF. We solve these problems using a uniform $20\times20\times1$ mesh with DPH20 elements, as well as using NASTRAN. The comparison between the meshes by NASTRAN (with 0.33 million DOFs) and the present method is shown in Fig. 19. The non-dimensional frequency parameter used for comparison is $\overline{\omega}_n = \omega_n a^2\sqrt{\rho_m h/D_m}$ in which $D_m = E_m h^3/12(1-v_m^2)$. The first six mode shapes along with the corresponding non-dimensional frequency parameters are shown in Figs. 20–22. Very good agreement is obtained for each of the different cases.

4 Conclusion

Through extensive numerical results of static and dynamic analyses of functionally-graded plates and shells, it is demonstrated that the proposed DPH20 and DPH27 elements are entirely capable of accurately and ef?ciently predicting the static and dynamical behaviors of FG structures in a very simple and cost-effective manner.

Because higher-order and layer-wise plate and shell theories involve (1) postulating very complex assumptions of plate/shell kinematics in the thickness direction, (2) defining generalized variables of displacements, strains, and stresses, and (3) developing very complex governing equilibrium, compatibility, and constitutive equations in terms of newly-defined generalized variables, while the currently proposed DPH20 and DPH27 elements merely involve displacement DOFs at each node, and rely only on the simple theory of solid mechanics, it is thus concluded by the authors that the development of higher-order or layer-wise theories are not entirely necessary for analyses of FG structures.

Acknowledgement: This research is supported by the Mechanics Section, Vehicle Technology Division, of the US Army Research Labs. The support of National Natural Science Foundation of China (grant No. 11502069) and Natural Science Foundation of Jiangsu Province (grant No. BK20140838) is also thankfully acknowledged.

References

Atluri, S. N. (2005): *Methods of Computer Modeling in Engineering and the Sciences*, Tech Science Press.

Batra, R. C.; Jin, J. (2005): Natural frequencies of a functionally graded anisotropic rectangular plate. *Journal of Sound and Vibration*, vol. 282, issue 1, pp. 509-516.

Carrera, E.; Brischetto, S.; Robaldo, A. (2008): Variable kinematic model for the analysis of functionally graded material plates. *AIAA Journal*, vol. 46, issue 1, pp. 194-203.

Carrera, E.; Brischetto, S; Cinefra, M.; Soave, M. (2011): Effects of thickness stretching in functionally graded plates and shells. *Composites Part B: Engineering*, vol. 42, issue 2, pp. 123-133.

Cheng, Z. Q.; Batra, R. C. (2000): Deflection relationships between the homogeneous Kirchhoff plate theory and different functionally graded plate theories. *Archives of Mechanics*, vol. 52, issue 1, pp. 143-158.

Dong, L.; El-Gizawy, A. S.; Juhany, K. A.; Atluri, S. N. (2014a): A simple locking-alleviated 4-node mixed-collocation finite element with over-integration, for homogeneous or functionally-graded or thick-section laminated composite beams. *CMC: Computers, Materials & Continua*, vol. 40, issue 1, pp. 49-77.

Dong, L.; El-Gizawy, A. S.; Juhany, K. A.; Atluri, S. N. (2014b): A simple locking-alleviated 3D 8-Node mixed-collocation C_0 finite element with over-integration, for functionally-graded and laminated thick-section plates and shells, with & without z-pins. *CMC: Computers, Materials & Continua*, vol. 41, issue 3,

pp. 163-192.

Dong, L.; Alotaibi, A.; Mohiuddine, S. A.; Atluri, S. N. (2014c): Computational methods in engineering: a variety of primal & mixed methods, with global & local interpolations, for well-posed or ill-Posed BCs. *CMES: Computer Modeling in Engineering & Sciences*, vol. 99, no. 1, pp. 1-85.

Fan, Q., Zhang, Y., Dong, L., Li, S., Atluri, S. N. (2015): Are Higher-Order Theories and Layer-wise Zig-Zag Theories Necessary for N-Layer Composite Laminates?. *CMES: Computer Modeling in Engineering & Sciences*, vol. 107, issue 2, pp. 155-186.

Ferreira, A. J. M.; Batra, R. C.; Roque, C. M. C.; Qian, L. F.; Martins, P. A. L. S. (2005): Static analysis of functionally graded plates using third-order shear deformation theory and a meshless method. *Composite Structures*, vol. 69, issue 4, pp. 449-457.

Hosseini-Hashemi, S.; Fadaee, M.; Atashipour, S. R. (2011a): Study on the free vibration of thick functionally graded rectangular plates according to a new exact closed-form procedure. Composite Structures, vol. 93, issue 2, pp. 722-735.

Hosseini-Hashemi, S.; Fadaee, M.; Atashipour, S. R. (2011b): A new exact analytical approach for free vibration of Reissner–Mindlin functionally graded rectangular plates. *International Journal of Mechanical Sciences*, vol. 53, issue 1, pp. 11-22.

Huang, C. S.; McGee, O. G.; Wang, K. P. (2013): Three-dimensional vibrations of cracked rectangular parallelepipeds of functionally graded material. *International Journal of Mechanical Sciences*, vol. 70, pp. 1-25.

Jin, G.; Su, Z.; Shi, S.; Ye, T.; Gao, S. (2014): Three-dimensional exact solution for the free vibration of arbitrarily thick functionally graded rectangular plates with general boundary conditions. *Composite Structures*, vol. 108, pp. 565-577.

Lo, K. H.; Christensen, R. M.; Wu, E. M. (1977): A high-order theory of plate deformation—part 2: laminated plates. *Journal of Applied Mechanics*, vol. 44, issue 4, pp. 669-676.

Matsunaga, H. (2008): Free vibration and stability of functionally graded plates according to a 2-D higher-order deformation theory. Composite structures, vol. 82, pp. 499-512.

Mindlin, R. D. (1951): Influence of rotatory inertia and shear on flexural motions of isotropic, elastic plates. *Journal of Applied Mechanics*, vol. 18, pp. 31–38.

Neves, A. M. A.; Ferreira, A. J. M.; Carrera, E.; Cinefra, M.; Roque, C. M. C.; Jorge, R. M. N.; Soares, C. M. M. (2013): Free vibration analysis of functionally graded shells by a higher-order shear deformation theory and radial basis functions

collocation, accounting for through-the-thickness deformations. *European Journal of Mechanics-A/Solids*, vol. 37, pp. 24-34.

Pradyumna, S.; Bandyopadhyay, J. N. (2008): Free vibration analysis of functionally graded curved panels using a higher-order finite element formulation. *Journal of Sound and Vibration*, vol. 318, no. 1, pp. 176-192.

Qian, L. F.: Batra, R. C.: Chen, L. M. (2004): Static and dynamic deformations of thick functionally graded elastic plates by using higher-order shear and normal deformable plate theory and meshless local Petrov–Galerkin method. *Composites Part B: Engineering*, vol. 35, issue 6, pp. 685-697.

Ramirez, F.: Heyliger, P. R.; Pan, E. (2006): Static analysis of functionally graded elastic anisotropic plates using a discrete layer approach. *Composites Part B: Engineering*, vol. 37, issue 1, pp. 10-20.

Reddy, J. N. (1984): A simple higher-order theory for laminated composite plates. *Journal of Applied Mechanics*, vol. 51, issue 4, pp. 745-752.

Reddy, J. N. (2000): Analysis of functionally graded plates. I*nternational Journal for Numerical Methods in Engineering*, vol. 47, issue 1-3, pp. 663-684.

Reddy, J. N. (2004): *Mechanics of laminated composite plates and shells: theory and analysis*, CRC press.

Reissner, E. (1945): The effect of transverse shear deformation on the bending of elastic plates. *Journal of Applied Mechanics*, vol. 12, pp. 69-77.

Thai, H. T.; Park, T.; Choi, D. H. (2013): An efficient shear deformation theory for vibration of functionally graded plates. *Archive of Applied Mechanics*, vol. 83(1), pp. 137-149.

Timoshenko, S.; Woinowsky-Krieger, S. (1959): *Theory of Plates and Shells*. McGraw hill, New York.

Yang, J.; Shen, H. S. (2003): Free vibration and parametric resonance of shear deformable functionally graded cylindrical panels. *Journal of Sound and Vibration*, vol. 261, no. 5, pp. 871-893.

Zenkour, A. M. (2006): Generalized Shear Deformation Theory for Bending Analysis of Functionally Graded Plates. *Applied Mathematical Modelling,* vol. 30, no. 1, pp. 67–84.

Zienkiewicz, O. C.; Taylor, R. L. (1977): *The finite element method (Vol. 3)*. London: McGraw-hill.

Zuo, H.; Yang, Z.; Chen, X.; Xie, Y.; Zhang, X. (2014): Bending, Free Vibration and Buckling Analysis of Functionally Graded Plates via Wavelet Finite Element Method. *CMC: Computers, Materials & Continua*, vol. 44, no. 3, pp. 167-204.